




Suitability of intravascular imaging for assessment of cerebrovascular diseases

S. Weigand^{1,2} · Sylvia Saalfeld^{2,3}  · T. Hoffmann^{1,2} · E. Eppler^{1,2} · T. Kalinski⁴ · K. Jachau⁵ · M. Skalej^{1,2}

Received: 18 February 2019 / Accepted: 21 May 2019 / Published online: 15 June 2019
© Springer-Verlag GmbH Germany, part of Springer Nature 2019

Abstract

Purpose Arteriosclerosis of the vascular system is associated with many accompanying diseases. Especially cerebral arteriosclerosis is a main risk factor for ischemic strokes. We want to verify the practicability of intravascular imaging like intravascular ultrasound and optical coherence tomography for the assessment of cerebral vessel walls and plaques.

Methods We examined 18 Circuli arteriosi willisii postmortem. The data contained 48 plaques from 48 different vessel parts. The samples underwent intravascular and histological imaging to conduct a quantitative assessment of vessel wall parameters (healthy vessel wall, thinnest vessel wall, plaque thickness and vessel diameter) as well as to qualitatively evaluate the healthy vessel wall, fibrotic plaques, calcifications and cholesterol deposits in diseased vessels.

Results The comparison showed statistically significant smaller measurements for thinnest vessel walls, normal vessel walls and vessel diameters in histology than in imaging. No statistically significant difference was reached for plaque diameters. Fibrotic plaques were characterized as hyper-intense with dorsal attenuation and calcifications as hypo-intense with dorsal attenuation in optical coherence tomography. In intravascular ultrasound, fibrotic plaques showed a homogeneous echogenicity without distal attenuation and calcifications were depicted as hyperechoic with dorsal sound shadows. Cholesterol deposits were hyper-intense in optical coherence tomography with strongly attenuated signals and in intravascular ultrasound; the deposits were hyper-intense with almost no attenuation.

Conclusion Both intravascular methods allow for plaque characterization and quantification of plaque diameter in cerebral vessel walls. When compared with histology, a statistically significant bias was obtained for the ex vivo measurements of the normal vessel wall diameters.

Keywords OCT · IVUS · Histology · Intracranial · Arteriosclerosis · Intravascular imaging

SW and SS contributed equally to this work.

✉ Sylvia Saalfeld
Sylvia.saalfeld@ovgu.de

- ¹ Department of Neuroradiology, University Hospital Magdeburg, Magdeburg, Germany
- ² Research Campus STIMULATE, Otto-von-Guericke University Magdeburg, Magdeburg, Germany
- ³ Department of Simulation and Graphics, University of Magdeburg, Magdeburg, Germany
- ⁴ Department of Pathology, University Hospital Magdeburg, Magdeburg, Germany
- ⁵ Institute of Forensic Medicine, University Hospital Magdeburg, Magdeburg, Germany

Introduction

Arteriosclerosis and accompanying diseases are the leading causes of death in industrialized countries [1]. In cardiology, intravascular ultrasound (IVUS) and optical coherence tomography (OCT) have been essential for intravascular imaging (IVI) of the vessel wall and evaluation of unstable plaques [2]. Arteriosclerosis of intracranial vessels accounts for 8–10% of ischemic strokes, and the use of IVI might also be helpful for diagnosis, prevention and treatment follow-up of cerebrovascular diseases, as it has been shown with coronary vessels [3]. However, IVI has not been clinically used for neurovascular diseases so far. The reasons are the more difficult intracranial access route as well as the small size and the unique structural composition of cerebral arteries [4].

OCT is a high-resolution imaging method with a spatial resolution of up to 10 μm, and it can assess stent struts and

arterial perforators, which remain undetected with angiography [5, 6]. Few neurovascular OCT experiments have been conducted on postmortem animal arteries or healthy human internal carotid arteries to date [7, 8]. In 2014, the first in vivo intravascular use of OCT was described to visualize a stent and a stent stenosis in the vertebrobasilar vessel [8]. In 2017, OCT was successfully conducted in a patient in vivo evaluating a stent malapposition showing one of the future applications of OCT in the management of intracerebral vascular pathologies [8, 9].

Concerning the feasibility of IVUS in intracranial arteries, only a few in vivo case reports exist. Pavlin-Premrl et al. were able to evaluate intracerebral arteriosclerosis in vivo when the catheter tip has been positioned in the correct place [10]. It also seems to aid in stent positioning [11]. Wehman et al. [12] used IVUS in two patients to assist the performance of intracranial angioplasty and stent placement in vivo. They demonstrated that it is possible to identify the proximal and distal extent of an arterial dissection, as well as to investigate the nature of the restenotic lesion. Overall, the potential benefit of their intracranial application is currently not approved and part of clinical practice for both methods [13]. Encouraged by the potential of IVUS and OCT in cardiology, the objective of our study was to prove and analyse the benefit of OCT and IVUS in order to assess the cerebrovascular wall and its pathologies.

Materials and methods

Sample data

The study comprises 18 samples of the circle of Willis (CoW), all acquired between September 2014 and April 2016 at the University Hospital of Magdeburg, with the approval of the local ethics committee. Due to the focus on vessel wall pathologies, patients with increased risk of cardiovascular diseases, such as adiposity, were selected. Specimens were acquired from 9 males and 9 females (average age at death: 61.8 ± 16.8 years). Since the study was completely exploratory, only a few criteria for the selection of the patients were created. For the withdrawal of the CoW, an equivalent gender proportion was respected. Only patients older than 50 years were selected. An exception to this was one cadaver of a 25-year-old corpse, which died due to a traffic accident. This provided a healthy CoW as a reference circulus. Other exceptions were cadavers who died because of subarachnoid haemorrhaging (one cadaver under 50 years). The maximum elapsed time between death and removal was 48 h. Data preparation revealed 48 plaques. All pathologies were evaluated with intravascular imaging and histology, yielding 851 slices available in at least 2 modalities (OCT, IVUS or histology) for quantitative evaluation and 64 structural attributes for qualitative evaluation.

Methods

The workflow was established through prior work [14] and is illustrated in Fig. 1. After removal and anatomical preparation, a 10-ml cannula was used to remove the remaining air and the circles were stored in 4% buffered formaldehyde solution for preservation (see Fig. 1(1) and 1(2)). Afterwards, the vessels were inspected by macroscopic examination and vessel wall pathologies were marked with needles (see Fig. 1(3) and 1(4)). The correct position was confirmed using an Olympus SZ61 stereo microscope (Shinjuku, Tokyo, Japan).

Next, intravascular imaging was carried out and the acquired data was analysed using the image processing software MeVisLab (MeVisLab, Version 2.7.1, MeVis Medical Solutions AG, Fraunhofer MEVIS, Bremen, Germany) (see Fig. 1(5)). Each vessel part was examined in detail using each modality (OCT and IVUS) twice to avoid and detect imaging artefacts. Due to the smaller diameter of the OCT catheter, thin vessel parts could only be probed with OCT. IVUS imaging was carried out with a standardised automated pullback device (Track Back II Device, Volcano Therapeutics Inc., Rancho Cordova, CA, USA) with a constant pullback velocity of 1.0 mm/s and an Eagle Eye platinum catheter (Volcano Therapeutics Inc., Rancho Cordova, CA, USA) with a probe diameter of 3.5 Fr. OCT was conducted using an “OPTISTM MOBILE” system (Abbott, Chicago, Illinois, USA) and the “LUNAWAVE” system (Terumo, Corporation, Shibuya, Japan). Both systems allow for a pullback length of 75 mm with a constant velocity of 36 mm/s. A DragonflyTM OPTISTM DUO Catheter (Abbott, Chicago, Illinois, USA) was employed with 2.7 Fr probe diameter.

For histological analysis, vessels and small bifurcating branches were cut perpendicularly to a maximum sample size of 10 mm. To mark the start and end of the vessel, two different ink colours were applied (see Fig. 1(6)) with additional longitudinal lines to ensure orientation, even in the event of any rotation from the histologic slicing. Before an ascending ethanol series and paraffin embedding, ink fixation was preserved by rinsing with acetic acid for 10 s. Plaques were serially cut with a slice distance of 500 μ m. For all samples, slice thickness was 2 μ m. After conventional haematoxylin-eosin (H&E) staining with an ST 5010 Autostainer XL (Leica Biosystems, Nussloch, Germany), digitalisation was carried out with the Hamamatsu Nanozoomer XR (Hamamatsu Photonics, Hamamatsu, Japan) (see Fig. 1(7)).

Cerebral arterial parts were evaluated quantitatively and pathologies were evaluated qualitatively based on OCT, IVUS and histological data (see Fig. 1(8)). For the identification of corresponding tissue parts, we used the needle-based landmarks. The needles caused artefacts in IVUS and OCT, which allowed for an easy co-registration of these markers. For each sample, the needles served as indicators, marking the beginning and end cutting points for histology. Furthermore,

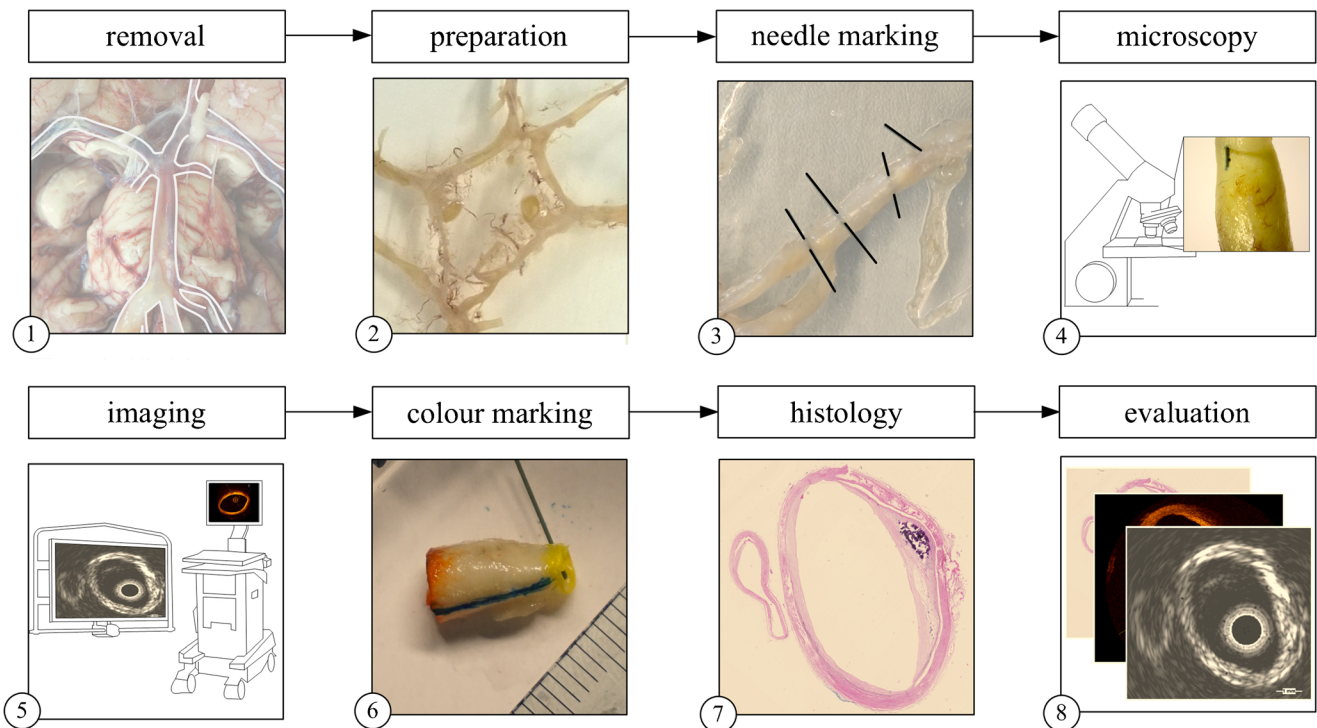


Fig. 1 Study workflow. After removing the circulus (1), preparation (2) and needle marking (3) was carried out. The needles and plaques were then evaluated with a microscope (4) to ensure the correct position of the needles. Subsequently, IVUS and OCT imaging (5) was done. Colour

marking (6) served as an orientation for histological analysis (7). For statistical and qualitative analysis, the intravascular images (5) and histologic slices (7) were correlated and compared (8).

orientation of the sample was made possible by colour inking, the ends and bifurcations of vessels. Based on constant pull-back velocities for intravascular imaging and constant histological slice distance, a co-registration was carried out, which was also controlled by manual inspection. For statistical analysis a paired *t* test as well as Pearson’s correlation coefficient were calculated with the statistical program SPSS (Version 24.0.0.0, Chicago, Illinois, USA).

In total, for 48 vessel wall parts and 48 plaques, the parameters x_{min} for thinnest vessel wall, x_{norm} for normal wall, x_p for plaque diameter and d_{max} for maximum vessel diameter were

extracted per slice, see Fig. 2. Qualitative analysis included a classification of the pathologic wall samples with respect to the signal intensity (S_{comp}), the signal’s homogeneity (S_{Homo}) and the pathology’s differentiation (*D*) compared with the healthy vessel wall. For each of the four pathologies, we classified its signal intensity S_{comp} in comparison with the healthy vessel wall (1-brighter, 0-similar, -1-darker, -2-no signal), the signal intensity’s homogeneity S_{Homo} (0 homogeneous, -1-signal intensity attenuation, -2-signal intensity extinction, x-heterogeneous) of the pathology and its possible differentiation *D* (2-complete differentiation, 1-pieewise differentiation, 0-no

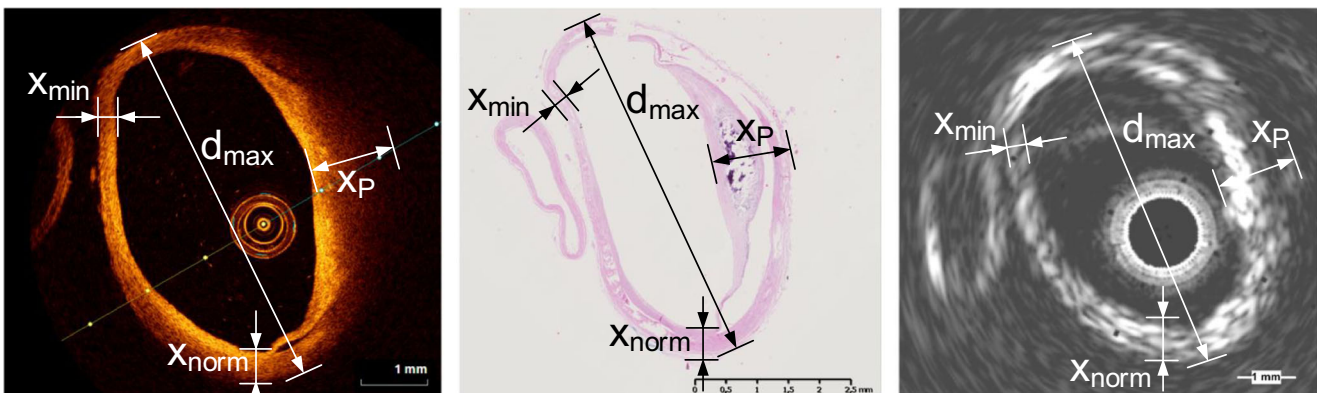


Fig. 2 Quantitative measurements of the vessel wall thickness; x_{min} for thinnest vessel wall, x_{norm} for normal wall, x_p for plaque diameter and d_{max} for vessel diameter

differentiation) from the healthy vessel wall. Qualitative classification was independently conducted by two experts. In case of disagreement, a third consensus analysis was carried out.

Results

Measurements of the cerebral vessel wall

During quantitative evaluation, 48 vessel parts containing 48 plaques were analysed. A further histologic classification of the plaques was not carried out for this step. The specific plaque locations are presented in Table 1. Overall, ten different vessel ramifications of the CoW were evaluated. The distribution shows a slightly higher proportion of the plaques in the larger intracranial vessels (e.g. vertebral artery, basilar artery and internal carotid artery). This is because of the higher prevalence of plaques in the larger intracranial vessels and the better suitability w.r.t. probing with intravascular catheters. We evaluated x_{norm} , x_{min} , d_{max} and x_p (Fig. 2). All results are summarized in Table 2. Overall, 215 slices, correlating in all three modalities, could be compared for quantitative assessment. Not all samples were measured and correlated using all three methods due to imaging artefacts and biological processes, e.g. intima detachments during postmortem fixations. Furthermore, traction forces of single-wall layers may have resulted in plaque detachments from the *tunica media*. To account for this, the distance of the detachment gap was subtracted from our measurements.

In the following, the quantitative comparisons for x_{norm} , x_{min} , d_{max} and x_p are reported by listing the results between the modalities. Also, the two modalities with the smallest disagreement are reported. For x_{norm} , the histological analysis yielded the smallest thickness values ($344 \pm 111 \mu\text{m}$) for 4 samples. OCT and IVUS exhibited an increased thickness, i.e. an average difference to histology of $10.6 \pm 9.3\%$ and $13.2 \pm 13.2\%$, respectively. Comparison of OCT and IVUS revealed an average difference of $3.9 \pm 11.0\%$.

Table 1 Specific localization of the plaques in the CoW

Localization	Absolute number	Relative percentage(%)
Left vertebral artery	5	10
Right vertebral artery	5	10
Basilar artery	13	27
Left posterior cerebral artery	2	4
Right posterior cerebral artery	1	2
Left internal carotid artery	6	13
Right internal carotid artery	7	15
Left middle cerebral artery	5	10
Right middle cerebral artery	3	6
Anterior communicating artery	0	0
Left anterior cerebral artery	0	0
Right internal carotid artery	1	2
Sum	48	100

Table 2 Left: quantitative results for measurement of healthy vessel walls x_{norm} , thinnest vessel wall x_{min} , maximum vessel diameter d_{max} and plaque thickness x_p with mean (M) and standard deviation (SD) values for the modalities histology (H), OCT and IVUS. Right: comparison of measurements of healthy vessel walls x_{norm} , thinnest vessel wall x_{min} , maximum vessel diameter d_{max} and plaque thickness x_p with mean (M) and standard deviation (SD) values for OCT vs. histology (OCT–H), IVUS vs. histology (IVUS–H) and IVUS vs. OCT (IVUS–OCT)

		<i>n</i>	M \pm SD (μm)			<i>n</i>	M SD (%)
x_{norm}	H	194	344 ± 111	OCT–H	194	10.6 ± 9.3	
	OCT	212	366 ± 107	IVUS–H	183	13.2 ± 13.2	
	IVUS	201	378 ± 107	IVUS–OCT	201	3.9 ± 11	
x_{min}	H	194	240 ± 81	OCT–H	194	14.2 ± 11.9	
	OCT	212	265 ± 87	IVUS–H	185	19.9 ± 24.5	
	IVUS	203	278 ± 94	IVUS–OCT	203	5.7 ± 16.3	
d_{max}	H	192	3794 ± 1038	OCT–H	191	-1.5 ± 15.8	
	OCT	211	3555 ± 935	IVUS–H	178	13.5 ± 19.2	
	IVUS	198	4174 ± 1037	IVUS–OCT	197	21.5 ± 26.4	
x_p	H	190	780 ± 301	OCT–H	190	1.8 ± 7.2	
	OCT	211	773 ± 310	IVUS–H	180	0.5 ± 12.7	
	IVUS	201	786 ± 304	IVUS–OCT	201	2.5 ± 19.5	

Similarly, values for x_{min} were smallest in histology ($240 \pm 81 \mu\text{m}$), followed by OCT ($264 \pm 87 \mu\text{m}$) and IVUS ($278 \pm 93.9 \mu\text{m}$). Differences between histology and OCT were smaller ($14.2 \pm 11.9\%$) than between IVUS and histology ($19.9 \pm 24.5\%$), and IVUS led to slightly larger values compared with OCT ($5.7 \pm 16.3\%$).

Values for d_{max} were largest in IVUS slices ($4174 \pm 1037 \mu\text{m}$), followed by histology ($3794 \pm 1038.4 \mu\text{m}$) and OCT ($3556 \pm 935 \mu\text{m}$). Our evaluation showed that measurements from OCT and histology were in agreement ($-1.4 \pm 15.8\%$), when compared with IVUS and histology ($13.4 \pm 19.2\%$) as well as IVUS and OCT ($21.5 \pm 26.3\%$).

For x_p , the three modalities led to measurements that were most similar. One hundred ninety plaques underwent histological analysis with an average thickness of $780 \pm 301 \mu\text{m}$. Only small differences were observed for OCT and histology ($1.8 \pm 7.2\%$), IVUS and histology ($0.5 \pm 12.7\%$) and IVUS and OCT ($2.5 \pm 19.5\%$).

In summary, the highest variability between modalities was observed for d_{max} and the lowest for x_p (Table 2.) Differences between OCT and IVUS were lower than when compared with histology. The histological measurements for x_{norm} and x_{min} were smaller than the intravascular ones.

The results of the statistical analysis are shown in Table 3. Pearson's correlation coefficient (r) yielded a strong correlation ($r \geq 0.8$) with statistical significance (p value < 0.01 two-sided) for all attributes in the pairwise comparisons (Table 3). A statistically significant difference for x_{norm} , d_{max} and x_{min} was obtained for all pairs (i.e. OCT vs. histology, IVUS vs. histology and IVUS vs. OCT), whereas x_p showed not only

Table 3 Test of paired samples for healthy vessel walls x_{norm} , thinnest vessel wall x_{min} , maximum vessel diameter d_{max} and plaque thickness x_p with mean (M) and standard deviation (SD). Correlation analysis based onPearson's correlation coefficient (r). Test statistics are denoted with (t) and degree of freedom (df) was 166 for all tests. p denotes the (two-sided) level of significance for both tests (*significance of 0.05 **significance of 0.01)

	Vessel part	M \pm SD	r	p	t	p
Histology–OCT	x_{norm}	-32.8 ± 36.7	.95	.00**	-11.57	.00**
	x_{min}	-31.8 ± 20.7	.97	.00**	-19.84	.00**
	d_{max}	104.7 ± 627.8	.8	.00**	2.16	.03*
	x_p	-9.6 ± 69.0	.97	.00**	-1.80	.07
Histology–IVUS	x_{norm}	-41.3 ± 45.5	.95	.00**	-11.72	.00**
	x_{min}	-43.7 ± 44.0	.97	.00**	-12.83	.00**
	d_{max}	-421.3 ± 552.6	.8	.00**	-9.85	.00**
	x_p	4.6 ± 128.7	.97	.00**	0.46	.65
OCT–IVUS	x_{norm}	-8.4 ± 29.7	.95	.00**	-3.66	.00**
	x_{min}	-12.0 ± 37.2	.97	.00**	-4.16	.00**
	d_{max}	-526.0 ± 609.3	.8	.00**	-11.16	.00**
	x_p	14.2 ± 132.9	.97	.00**	1.38	.17

strong correlation but also strong accuracy with no statistical significance when comparing OCT vs. histology ($p = 0.073$), histology vs. IVUS ($p = 0.65$) and IVUS vs. OCT ($p = 0.17$).

Characterization of the vessel wall pathologies

All three modalities were able to depict the three vessel layers: the *tunica intima*, *tunica media* and *tunica adventitia* (Fig. 3). IVUS and OCT mapped the *tunica intima* as hyper-intense, the *tunica media* as hypo-intense and the *tunica adventitia* as brighter than the *tunica media*. Since the *tunica media* represents the largest part of the vessel wall, it was used as a reference for the evaluation of pathological changes. The absolute and relative percentages of the signal description characterizing the pathologies are summarized in Table 4.

When examining the histological images of the 48 plaques, 44 of them could be identified as fibrotic. The remaining four

plaques could not be clearly categorized as fibrotic plaques due to their widely varying components. Furthermore, we found cholesterol deposits in 8 of the 48 plaques yielding 8 cholesterol deposits for the qualitative evaluation. In addition, we found calcifications in 9 of the 48 plaques.

All of the 44 fibrotic plaque samples could be assessed with OCT. In IVUS images, only 42 of the fibrotic plaques could be evaluated. Histological analysis identified the fibrotic plaques as fibrotic tissue growth between the *tunica media* and the endothelium. OCT yielded a homogeneous and brighter signal compared with the vessel wall, while in IVUS, an iso-intense signal was noticed (Fig. 4). Fibrotic plaques showed a dorsal attenuation in OCT, whereas in IVUS, no dorsal attenuation occurred. Differentiation of the fibrotic plaques could be better carried out in OCT than in IVUS.

We evaluated 9 plaques with macro-calcifications. For the evaluation of calcifications, histological analysis revealed

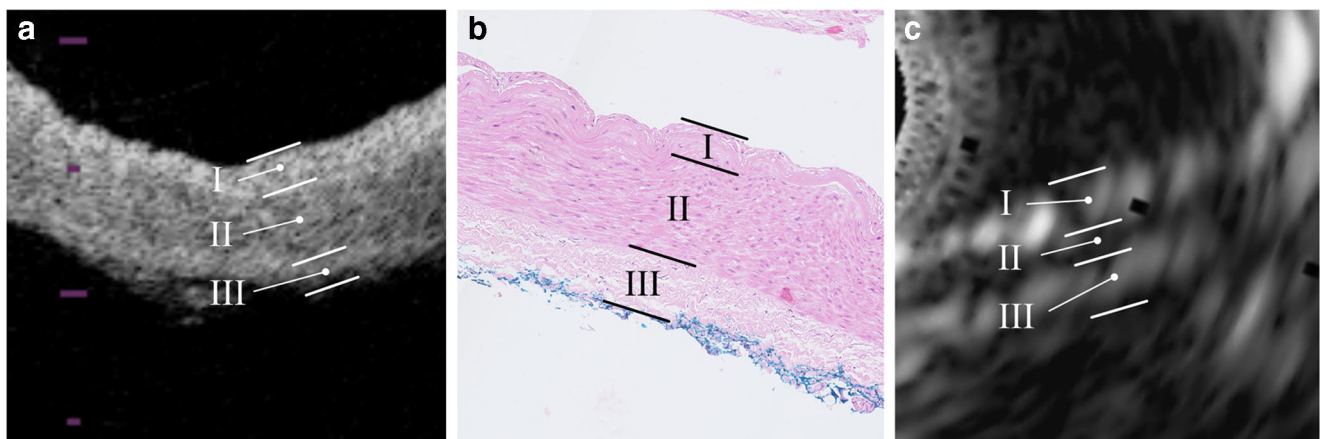


Fig. 3 Assessment of the three vessel wall layers by **a** OCT, **b** HE-stained histological slide and **c** IVUS. The *tunica intima* (I) and *tunica adventitia* (III) were characterized as hyper-intense area and the *tunica media* (II) as

hypo-intense area in OCT (**a**) and IVUS (**c**). Note the blue colour ink marking at the outer surface of the *tunica adventitia* in the histological image (**b**)

Table 4 Qualitative analysis of the evaluated structures. We classified the signal intensity S_{comp} in comparison with the healthy vessel wall (1-brighter, 0-similar, -1-slightly darker, -2-darker), the signal intensity's homogeneity S_{homo} (0-homogeneous, -1-signal intensity attenuation, -2-signal intensity extinction, x-heterogeneous) and the differentiation D (2-complete

differentiation, 1-piecewise differentiation, 0-no differentiation) from the pathologies' environment. In the first row of each evaluated structure type, the absolute number and in the second row, the relative number of frequency occurrences are provided

	$S_{compOCT}$				$S_{homoOCT}$				D_{OCT}		
	1	0	-1	-2	0	-1	-2	X	2	1	0
Healthy vessel wall	–	–	–	–	3/3	–	–	–	3/3	–	–
3 OCT	–	–	–	–	100%	–	–	–	100%	–	–
Fibrotic plaque	34/44	10/44	–	–	9/44	35/44	–	–	21/44	23/44	–
44 OCT	77.3	22.3%	–	–	20.4%	79.5%	–	–	47.7%	52.3%	–
Calcifications	–	–	9/9	–	–	6	2	1	3/9	6/9	–
9 OCT	–	–	100%	–	–	66.7%	22.2%	11.1%	33.3%	66.7%	–
Cholesterol deposits	8/8	–	–	–	1/8	2/8	5/8	–	6/8	2/8	–
8 OCT	100%	–	–	–	12.5%	25%	63.5%	–	75%	25%	–
	$S_{compIVUS}$				$S_{homoIVUS}$				D_{IVUS}		
	1	0	-1	-2	0	-1	-2	X	2	1	0
Healthy vessel wall	–	–	–	–	2/3	–	–	1/3	2/3	1/3	–
3 IVUS	–	–	–	–	66.7%	–	–	33.3%	66.7%	33.3%	–
Fibrotic plaque	7/42	29/42	6/42	–	35/42	1/42	–	6/42	12/42	30/42	–
42 IVUS	16.7%	69.1%	14.3%	–	83.3%	2.4%	–	14.3%	28.6%	71.4%	–
Calcifications	8/8	–	–	–	4/8	2/8	–	2/8	6/8	2/8	–
8 IVUS	100%	–	–	–	50%	25%	–	25%	75%	25%	–
Cholesterol deposits	6/8	2/8	–	–	7/8	1/8	–	–	6/8	2/8	–
8 IVUS	75%	25%	–	–	87.5%	12.5%	–	–	75%	25%	–

blue/violet parts that were well differentiated and mostly located in the basal or central part of the fibrotic plaques (Fig. 5) [15]. In OCT, they exhibited hypo-intense signals with dorsal attenuations and distinct delineation. IVUS was able to detect only 8 out of 9 calcifications. The remaining one was represented mostly hyper-intense with varying dorsal attenuation and distinct differentiation.

In addition to the fibrotic plaque, cholesterol deposits are shown in Fig. 5. Eight cholesterol deposits could be evaluated. In the histological images, cholesterol cavities are present. OCT revealed the cholesterol deposits hyper-intense with a signal attenuation or extinction behind them and distinct delineation. IVUS showed slightly increased signal intensity

with much less dorsal signal attenuation and distinct delineation.

Discussion

The statistical analysis of the quantitative analysis showed a strong correlation with high correlation coefficients ($r \geq 0.8$) between the three measurement procedures for all vessel parameters. Because of the high statistical significant r values, clinical conclusions can be drawn independent of its accuracy in terms of micrometre. The measurements of the cerebral vessel wall dimensions revealed a pairwise statistically

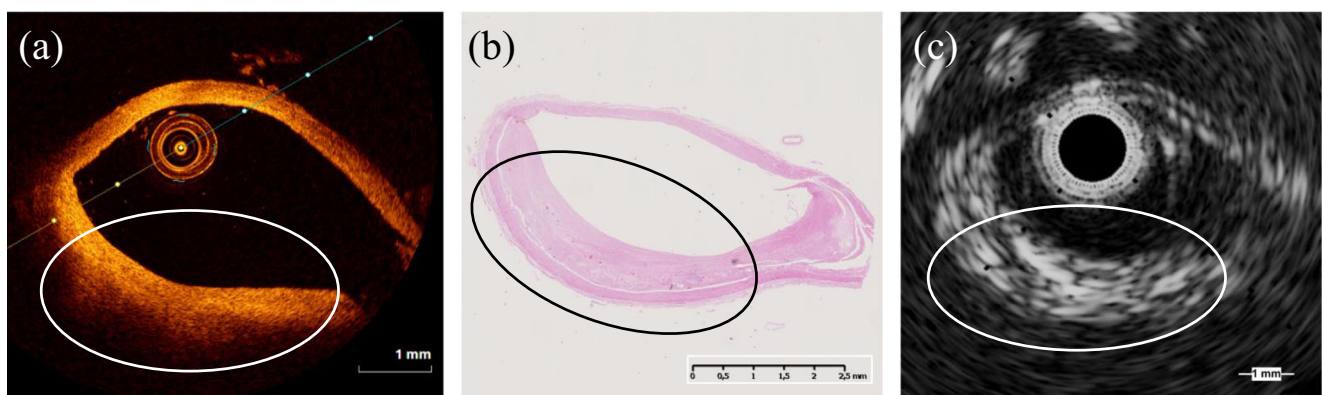


Fig. 4 Depiction of fibrotic plaque between *tunica intima* and *tunica media* in **a** OCT, **b** HE-stained histological slides and **c** IVUS. In OCT (**a**), fibrotic plaques are hyper-intense (see ellipse) with dorsal signal

attenuation, and in IVUS (**c**), fibrotic plaques are iso-intense plaque areas compared with the normal vessel wall without dorsal signal attenuation

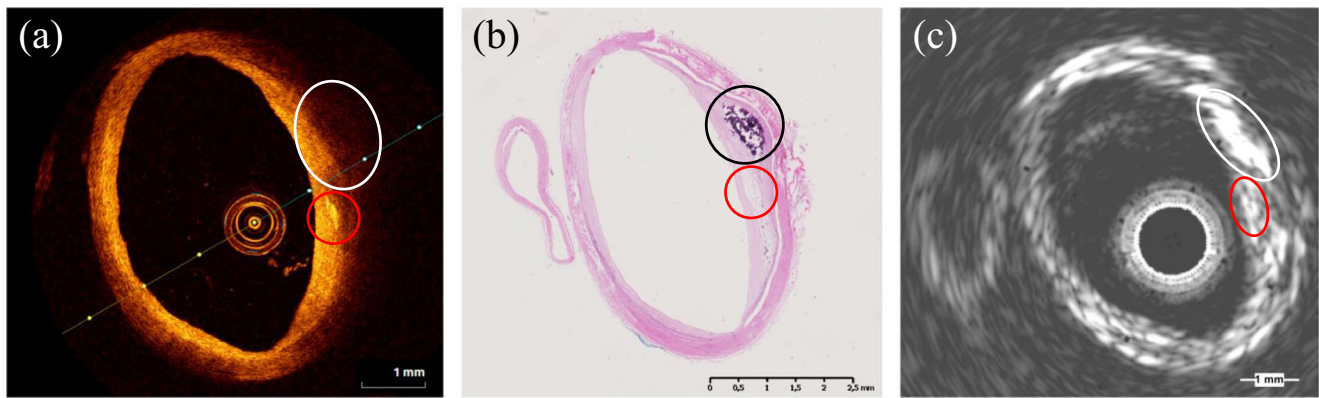


Fig. 5 Calcifications (white and black circles) and cholesterol deposits (red circle) inside a fibrotic plaque as depicted by **a** OCT, **b** HE-stained histological slide and **c** IVUS. OCT (**a**) identified calcifications as hypo-intense with dorsal signal attenuation. Histological analysis (**b**) yielded blue-violet coloured calcification (black circle) next to the cholesterol deposits (red circle) within the plaque. IVUS (**c**) depicted calcifications

as hyper-intense with varying dorsal signal attenuation. Cholesterol deposit-caused cavities (red circle) in a fibrotic plaque are visible by histology (**b**). OCT (**a**) shows distinct delineated hyper-intense regions. IVUS (**c**) revealed a slightly increased signal intensity with distinct delineation

significant bias between OCT, IVUS and histology for x_{\min} , x_{norm} and d_{\max} , but not for x_p . This underlines the excellent possibility for intravascular imaging in plaque measuring. Possible reasons include the high-quality delineation of plaques, as well the almost non-existent shrinkage of fibrotic tissue and plaques, by loss of water during histological fixation due to the already reduced water content. The large variations of the maximum vessel diameter d_{\max} (up to 43.3%) may be caused by the natural variations of the cerebral vessels and deformations during probing with the catheter. The statistically significant bias between OCT and IVUS for x_{\min} and x_{norm} is contradictory to related work reporting correlations for larger vessels like coronary arteries [16, 17]. This could be due to the small sizes of cerebral vessels. x_{\min} measurements were small in OCT (265 μm) and histology (240 μm), i.e. near the maximum possible axial resolution of IVUS (170 μm), resulting in an overestimation of vessel wall thickness in IVUS. In summary, the results for x_p make a strong case for intravascular imaging to characterize cerebral plaques and are in agreement with the literature [13].

The characterization of the vessel wall pathologies, with respect to signal intensities and differentiation, matches related studies evaluating coronary arteries [13, 17, 18]. OCT was able to differentiate fibrotic plaques, whereas IVUS imaging sometimes missed fibrotic plaques due to its lower differentiation to the healthy vessel wall. In general, OCT showed fibrotic plaques brighter than the healthy vessel wall, but was often accompanied by dorsal signal attenuation. For increased plaque thickness, OCT's signal distinction is caused due to the smaller penetration depth. Both intravascular imaging methods revealed calcifications and cholesterol deposits. Since larger calcifications were detected more easily, we analysed macro-calcifications, which were depictable with IVUS' resolution. Delineation of calcifications was possible with OCT and IVUS. OCT yielded hypo-

intense signal intensities with dorsal intensity attenuation, whereas IVUS yielded hyper-intense signal intensity with increased signal attenuation. Regarding cholesterol deposits, OCT was inferior to IVUS due to the larger dorsal attenuation. Surrounding macro-calcifications complicated the evaluation due to the strong signal loss, which was also reported by Di et al. [19]. In literature, plaques with homogeneous cholesterol components are often declared as lipid plaques and are evaluated as a whole. Studies report superior differentiation between lipid and fibrotic plaques for OCT compared with IVUS [18]. However, the cholesterol deposits, also called lipid pools, are hypo-intense and are not well-differentiated areas in literature for extra-cerebral vessels [13, 17, 18]. This is in contrast to our results, where the signal intensity of the fibrotic plaque showed a mix of hyper-intense ($S_{\text{comp}}(\text{OCT}) = 1$) and iso-intense ($S_{\text{comp}}(\text{OCT}) = 0$) signals, whereas all cholesterol deposits presented a hyper-intense signal in OCT ($S_{\text{comp}}(\text{OCT}) = 1$). A reason for this misalignment might be a difference in approach to evaluation (i.e. evaluating lipid plaques as a whole vs. evaluating the cholesterol deposits). In accordance with the literature, a distinct delineation of cholesterol deposits was possible during intravascular imaging.

A central limitation of our study is the ex vivo sample preparation, since OCT and IVUS are currently not approved for use in cerebral arteries. Degradative intracellular processes occur because of postmortem tissue changes, which can happen during the time between death and sample preparation. An attempt was made to minimize the impact of this process by setting the maximum time between death and preparation of the Circle of Willis at 48 h. In the histological analysis, intima and plaque detachment prevented exact histological measurements. Finally, signal distinctions in OCT and IVUS partially prevented the plaque assessment and had a resulting impact on statistical evaluation. Moreover, the number of pathologies was rather low since each pathology was only evaluated in

one slice to prevent statistical bias. Overall, the study demonstrated the practical applications of OCT and IVUS in an *in vitro* setting to evaluate the healthy and the arteriosclerotic wall of intracranial arteries. Interestingly, Wehman et al. [12] used IVUS in two patients *in vivo*, and Gounis et al. [20] recently introduced the high-frequency (HF) OCT and a prototype, which is already in preclinical testing. Thus, we expect that HF OCT will be for clinical use in the near future.

The presented study showed that measuring the plaque diameter with IVI yielded no statistically significant difference to the histologically determined measurements. Furthermore, it is possible to assess the structure of the plaque in intracranial vessels with IVUS and OCT. This might be beneficial for a classification of intracranial plaques into stable and unstable and thus a high or low rupture risk can be assigned. Hence, strokes may be prevented which are caused by unstable plaques. So for future strategies, a precise assessment of intracranial plaques and their rupture risk could bring new guidelines for diagnosis and treatment of intracranial arteriosclerosis.

For extracranial arteries, e.g. the carotid artery, a prospective study with IVUS-Virtual Histology (IVUS–VH) was conducted in 119 patients, providing qualitative and quantitative compositions of the carotid plaque [21]. In accordance with our study with intracranial vessels, IVUS–VH could accompany the imaging of intracranial vessels and provide additional information. Further research is needed to identify those pathologies and findings in diseased intracranial vessels which correlate with the incidence of ischemic strokes and thromboembolic events. In coronary artery disease, a thin-cap fibroatheroma is a sign of a vulnerable plaque and the evidence points towards the risk of plaque rupture, the major mechanism for sudden coronary artery occlusion [22]. Because of the differences in structure and small size, there might be other mechanisms in intracranial arteries that lead to thrombosis and vessel occlusion, so findings in coronary arteries cannot be directly related to intracranial vessels. It is important to further evaluate these mechanisms, in order to decide which modality should be technically improved for safe access to intracranial vessels *in vivo*. There are clear technical advantages for OCT, such as the thinner catheters and the higher resolution by underlying physical principles, which are better suited to the dimensions of small intracranial arteries and vessel walls.

Conclusion

Eighteen circles of Willis' including 48 plaques, 9 calcifications and 8 cholesterol deposits were evaluated by correlating IVUS, OCT and histology. The findings reveal the ability of intravascular imaging to characterize cerebral vessels and their pathologies. Both OCT and IVUS allow for plaque characterization and quantification of plaque diameter.

OCT has a superior resolution, which is beneficial for characterization of wall pathologies, but the limited penetration depth prevents the assessment of the complete vessel wall. Advantages of IVUS include the increased penetration depth and its proven clinical applications. On the contrary, a lower resolution complicates plaque evaluation, plus catheter diameters as well as acquisition time are higher than for OCT.

In conclusion, a complete evaluation of cerebral pathologies would include a combination of various imaging modalities. Intravascular imaging will have an increasingly important role in the future as non-invasive methods are not able to depict the vessel wall at sufficient resolution. However, additional research and development is needed to develop more flexible and thinner catheters to navigate physical barriers such as carotid syphons or strongly bent cerebral vessel parts.

Funding This study was funded by the Federal Ministry of Education and Research in Germany within the Research Campus STIMULATE (13GW0095A) and the German Research Foundation (SA 3461/2-1).

Compliance with ethical standards

Conflict of interest The authors declare that they have no conflict of interest.

Ethical approval All procedures performed in studies involving human participants were in accordance with the ethical standards of the institutional and/or national research committee and with the 1964 Helsinki declaration and its later amendments or comparable ethical standards.

Informed consent Informed consent was obtained from all individual participants included in the study.

References

- Osborn EA, Jaffer FA (2013) Imaging atherosclerosis and risk of plaque rupture. *Curr Atheroscler Rep* 10(15):359
- Segura T, Serena J, Castellanos M, Teruel J, Vilar C, Davalos A (2001) Embolism in acute middle cerebral artery stenosis. *Neurology*. 56:497–501
- Andrus EC, Allen EV, Merritt HH, Duff GL, Moore RA, Kendall FE et al (2015) The pathogenesis of arteriosclerosis. *Int J Epidemiol* 44(6):1791–1793
- Standish BA, Spears J, Marotta TR, Montanera W, Yang VX (2012) Vascular wall imaging of vulnerable atherosclerotic carotid plaques: current state of the art and potential future of endovascular optical coherence tomography. *AJNR*. 33(9):1642–1650
- Fujimoto JG, Pitris C, Boppart SA, Brezinski ME (2000) Optical coherence tomography: an emerging technology for biomedical imaging and optical biopsy. *Neoplasia* 2(1):9–25
- Mathews MS, Su J, Heidari E, Levy EI, Linskey ME, Chen Z (2011) Neuroendovascular optical coherence tomography imaging and histological analysis. *Neurosurgery*. 69(2):430–439
- Lopes DK, Johnson AK (2012) Evaluation of cerebral artery perforators and the pipeline embolization device using optical coherence tomography. *J Neurointerv Surg*, neurintsurg-2011-010102 4: 291–294

8. Chen CJ, Kumar JS, Chen SH, Ding D, Buell TJ, Sur S et al (2018) Optical coherence tomography: future applications in cerebrovascular imaging. *Stroke*. 49(4):1044–1050
9. Given CA, Ramsey CN, Attizzani GF, Jones MR, Brooks WH, Bezerra HG et al (2015) Optical coherence tomography of the intracranial vasculature and Wingspan stent in a patient. *J Neurointerv Surg* 7(6):e22
10. Pavlin-Premrl D, Sharma R, Campbell BC, Mocco J, Opie NL, Oxley TJ (2017) Advanced imaging of intracranial atherosclerosis: lessons from interventional cardiology. *Front Neurol* 8(387):387
11. Hussain AS, Hussain NS (2016) Intravascular ultrasound for intracranial and extracranial carotid artery stent placement. *Cureus*. 8:8
12. Wehman JC, Holmes DR Jr, Hanel RA, Levy EI, Hopkins LN (2006) Intravascular ultrasound for intracranial angioplasty and stent placement: technical case report. *Neurosurgery*. 59(Suppl 2):ONS-E481-3
13. Farooq MU, Khasnis A, Majid A, Kassab MY (2009) The role of optical coherence tomography in vascular medicine. *Vasc Med* 14(1):63–71
14. Hoffmann T, Glaßer S, Boese A, Brandstädter K, Kalinski T, Beuing O, Skalej M (2016) Experimental investigation of intravascular OCT for imaging of intracranial aneurysms. *Int J Comput Assist Radiol Surg* 11(2):231–241
15. Lee RT, Grodzinsky AJ, Frank EH, Kamm RD, Schoen FJ (1991) Structure-dependent dynamic mechanical behavior of fibrous caps from human atherosclerotic plaques. *Circulation*. 83(5):1764–1770
16. Kubo T, Akasaka T, Shite J, Suzuki T, Uemura S, Yu B et al (2013) OCT compared with IVUS in a coronary lesion assessment: the OPUS-CLASS study. *JACC Cardiovasc Imaging* 6(10):1095–1104
17. Yabushita H, Bouma BE, Houser SL, Aretz HT, Jang IK, Schlendorf KH, Kauffman CR, Shishkov M, Kang DH, Halpern EF, Tearney GJ (2002) Characterization of human atherosclerosis by optical coherence tomography. *Circulation*. 106(13):1640–1645
18. Jang IK, Bouma BE, Kang DH, Park SJ, Park SW, Seung KB, Choi KB, Shishkov M, Schlendorf K, Pomerantsev E, Houser SL, Aretz HT, Tearney GJ (2002) Visualization of coronary atherosclerotic plaques in patients using optical coherence tomography: comparison with intravascular ultrasound. *J Am Coll Cardiol* 39(4):604–609
19. Di LV, Imola F, Gatto L, Romagnoli E, Limbruno U, Marco V et al (2017) Limitations of OCT in identifying and quantifying lipid components: an in vivo comparison study with IVUS-NIRS. *EuroIntervention*. 13(3):303–311
20. Gounis MJ, Ughi GJ, Marosfoi M, Lopes DK, Fiorella D, Bezerra HG, Liang CW, Puri AS (2019) Intravascular optical coherence tomography for neurointerventional surgery. *Stroke* 50(1):218–223
21. Sangiorgi G, Bedogni F, Sganzerla P, Binetti G, Inglese L, Musialek P, Esposito G, Cremonesi A, Biasi G, Jakala J, Mauriello A, Biondi-Zoccai G (2013) The Virtual histology In CaroTids Observational Registry (VICTORY) study: a European prospective registry to assess the feasibility and safety of intravascular ultrasound and virtual histology during carotid interventions. *Int J Cardiol* 168(3):2089–2093
22. Virmani R, Kolodgie FD, Burke AP, Farb A, Schwartz SM (2000) Lessons from sudden coronary death: a comprehensive morphological classification scheme for atherosclerotic lesions. *Arterioscler Thromb Vasc Biol* 20(5):1262–1275

Publisher's note Springer Nature remains neutral with regard to jurisdictional claims in published maps and institutional affiliations.